단결정 압전섬유작동기를 사용한 능동 비틀림 로터 블레이드의 최적 설계 및 진동하중 해석

Design optimization and vibratory loads analysis of active twist rotor blades incorporating single crystal piezoelectric fiber composites

박재상† ·신상준*
JaeSang Park and SangJoon Shin

Key Words : Single crystal piezoelectric fiber composites, Active twist rotor blades, Design optimization, Vibratory loads reduction

ABSTRACT

This paper presents a design optimization of a new Advanced Active Blade Twist (AATR-II) blade incorporating single crystal Macro Fiber Composites (MFC) and conducts vibratory loads reduction analysis using an obtained optimal blade configuration. Due to the high actuation performance of the single crystal MFC, the AATR blade may reduce the helicopter vibration more efficiently even with a lower input-voltage as compared with the previous ATR blades. The design optimization provides the optimal cross-sectional configuration to maximize the tip twist actuation when a certain input-voltage is given. In order to maintain the properties of the original ATR blade, various constraints and bounds are considered for the design variables selected. After the design optimization is completed successfully, vibratory load reduction analysis of the optimized AATR-II blade in forward flight condition is conducted. The numerical result shows that the hub vibratory loads are reduced significantly although 20% input-voltage of the original ATR blade is used.

1. Introduction

Vibration and noise reduction are two primary objects of the present investigation in helicopters. The high levels of vibration and noise cause serious constraints such as relatively poor ride quality, restricted flight envelope, low fatigue life of the structural components, and the resultant high operating cost. The primary source of these problems is the complex unsteady aerodynamic environment which is generated near the rotor blades mainly during forward flight.

In order to relieve such problems, recently, active control methodologies using piezoelectric materials have been examined. These approaches modify directly the periodic aerodynamic loads acting upon the rotor blades. One of active rotor controls is the Active Twist Rotor (ATR, Figure 1).

The ATR blade utilizes piezoelectric fiber composite actuators (Figure 2) such as Active Fiber Composites (AFC, [1]) or Macro Fiber Composites (MFC, [2]) that are embedded directly within the composite blade skin. These actuators produce strain-induced twisting deformations of the blade, when activated by electrical voltage.

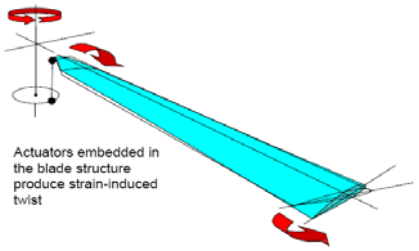

Figure 1. Active Twist Rotor blades

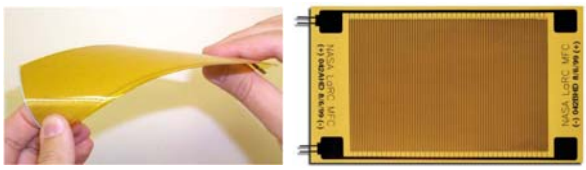

Figure 2. AFC (Left) and MFC (Right)

Under the NASA/Army/MIT ATR program [3-7] up to 2003, the ATR blade using AFC was designed, manufactured and tested successfully. An ATR prototype blade was designed and fabricated for bench and hover tests [3, 4]. After minor design modification, a set of ATR blades were manufactured, analyzed and wind-tunnel-tested in forward flight condition [5, 6]. As a result, during the open-loop forward flight test, significant vibration reduction on both fixed- and rotating-system loads was achieved. Finally, a closed-loop controller was designed to reduce the ATR hub

† 서울대학교 기계항공공학부, 박사후 연구원
E-mail : tux2000@snu.ac.kr
Tel : (02) 880-1901, Fax : (02) 887-2662
* 서울대학교 기계항공공학부, 조교수

shear vibratory loads and implemented successfully in the Langley wind tunnel experimental setup [7].

Following the completion of the ATR program, the U.S. Army Research Laboratory Vehicle Technology Directorate initiated a study on advanced blade design techniques for the Advanced ATR (AATR) blade [8] using MFC. The original ATR blade was designed to have a rectangular blade planform and a NACA 0012 airfoil in order to reduce the blade design complexity. However, the AATR blade uses the high performance airfoil and advanced blade tips.

Although ATR blades utilizing AFC or MFC have been designed successfully, most of them were designed by the manually-driven iterative process, which did not guarantee a theoretical optimum design. Only one example [9] for an optimal design of the ATR blade was found in the literature and it presented an optimized cross-section configuration of the AATR blade to maximize the twist actuation.

Even though ATR blades incorporating AFC or MFC could reduce significantly vibration and acoustic noise of helicopters, a quite high input-voltage (2,000 V_{pp}) was unavoidably required.

The single crystal piezoelectric materials [10] can produce strain levels more than 1% and exhibit five times larger than that of the conventional piezoceramic materials in terms of strain energy density. In addition, they have higher coupling constants. Although it is still difficult to manufacture the single crystal piezoelectric materials in large quantities and complex geometries, it will be advantageous to use the improved actuation performance of the piezoelectric fiber composites [11, 12].

In this paper, it is suggested to conduct design optimization and vibration load reduction analysis in forward flight of a new AATR blade (AATR-II) incorporating the MFC using single crystal piezoelectric materials, PMN-32%PT [13]. This new blade is expected to consume much lower input-voltage when compared with previous ATR blades. The AATR-II blade will be designed based on the AATR blade configuration, which originally uses the standard MFC, but to maintain the properties of the original ATR blade. The goal of the design optimization will be to find the cross-section configuration which produces the maximum twist actuation when a certain input-voltage is provided. After the design optimization is completed successfully, the hub vibratory loads reduction performance of the optimized AATR-II blade in forward flight will be investigated and the result will be compared with the experimental result of the original ATR blade.

2. Formulation

2.1 Description of the problem

The optimization problem to maximize the twist actuation of the AATR-II blade can be expressed as

$$\max_{x} f(x) \tag{1}$$

subject to

$$g(x) \le 0 \tag{2}$$

$$x_l \le x \le x_u \tag{3}$$

where f is an objective function which is the static tip twist due to the actuation of the single crystal MFC and x is a vector of the design variables. In addition, $g(x)$ is the set of nonlinear constraints, x_l and x_u are lower and upper bounds of x, respectively.

2.2 Design variables

In this paper, as shown in Figure 4, the design variables for the optimization problem are as follows.

- Starting and ending locations of the active region
- Chordwise location of the web
- Length of the web extension
- Two discrete ballast weights with their masses and chordwise locations

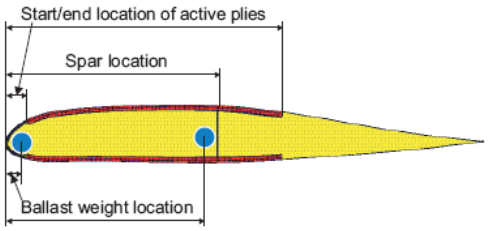

Figure 4. Design variables for the optimal design of the AATR-II blade

The blade planform is divided into four spanwise sections of predetermined length as shown in Figure 5. Each section uses a different advanced airfoil; the first section has RC-412, the second section has RC-410, and the other sections have RC-608. For first three most inboard sections, the same design variables are used. The most outboard section is the blade tip and it has the tip droop/sweep as an additional variable. Its cross-sectional layup is a continuous extension from the neighboring inboard section. However, from the manufacturing constraints, the chordwise location of the web needs to be a single design variable along the whole blade span.

Finally, each design variable should have the permissible range.

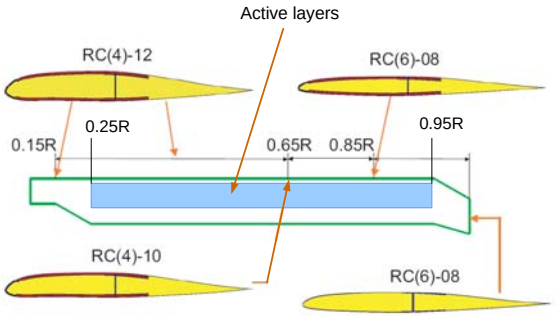

Figure 5. Planform and cross-section geometry of the AATR-II blade (R=1.397 m)

2.3 Constraints

For aeroelastic stability, structural integrity, unique structural characteristics, and in order to match Lock number, various constraints, $g(x)$, need to be included as follows.

- Chordwise location of the cross-sectional center of gravity (for aeroelastic stability)
- Chordwise location of the cross-sectional elastic axis (for aeroelastic stability)
- Blade mass per unit span length (to match Lock number)
- Blade fundamental rotating frequencies (for desirable blade dynamics)
- Maximum allowable blade local strain under the worst-case loading condition (structural integrity)

2.4 Design optimization framework

In order to perform design optimization, various numerical design and analysis tools are used. Figure 6 shows the design optimization framework to maximize the tip twist actuation of the AATR-II blade.

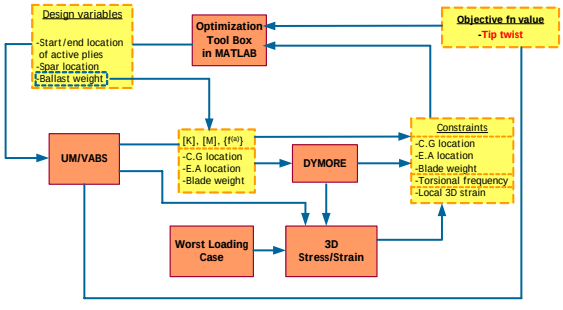

Figure 6. Design optimization framework of the AATR-II blade

MATLAB [14] provides an environment to integrate different analysis tools and conducts design optimization. In this paper, the three-dimensional (3-D) blade analysis is separated into two-step analyses, i.e., two-dimensional (2-D) linear cross-section analysis and one-dimensional nonlinear (1-D) beam analysis. After determining initial sectional properties from the cross-section analysis, they will be substituted into the beam analysis. For the cross-section and beam analyses, UM/VABS (University of Michigan Variational-Asymptotic Beam Cross-Sectional Analysis, [15]) and DYMORE [16] are used, respectively. In addition, the cross-sectional parametric mesh generator for UM/VABS and 3-D strain module are applied.

UM/VABS performs 2-D cross-sectional analysis of beams using finite element method (FEM) and provides sectional-stiffness, inertial properties and actuation force/moments which are used in the beam analysis. Furthermore, it calculates blade mass per unit span length, cross-sectional locations of the center of the gravity and elastic axis, and static active deformation of the cross-section.

After the 2-D cross-section analysis is completed, 1-D global blade analysis is conducted by a multibody dynamics code, DYMORE, which is developed by Bauchau. DYMORE provides an exact solution of the geometrically nonlinear beam. In the present design framework, DYMORE calculates the natural frequencies and centrifugal loads of the blade at normal rotating condition.

When the blade properties and loads are given, 3-D strain module computes internal 3-D strain/stress distribution. In order to obtain the most conservative design load, the maximum forward flight speed condition is selected as the worst loading case in this paper. The worst case sectional blade loads for flapwise bending, chordwise bending, and torsion, which are obtained from CAMRAD-II simulation in the previous ATR program, are adopted and the centrifugal loads are added to those worst case loads. For each calculated strain component, the maximum strain criterion is applied and compares it with the allowable of the local constituent material.

Finally, the function 'fmincon' of MATLAB optimization toolbox conducts a mathematical optimization. This function is a gradient based method that attempts to find a constrained minimum of a scalar function of multiple variables staring at an initial estimate. This is generally referred to as constrained nonlinear optimization. Three kinds of termination criteria are provided: the maximum number of iteration, tolerance on the design variables, and tolerance on the function value. When one of these termination criteria is satisfied, the optimization loop will be finished.

2.5 Forward flight analysis model

In this work, through direct time integration, DYMORE performs the forward flight response of the optimized AATR-II blade due to the actuation of the single crystal MFC. Figure 7 shows the analysis model of the four-active-bladed AATR-II system for the forward flight time domain analysis.

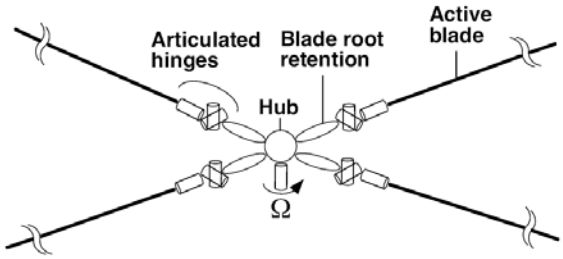

Figure 7. Detailed multi-body modeling of 4-active-bladed AATR-II system

The hub is modeled as a rigid body, and connected with a revolute joint underneath. It is under a prescribed rotation with nominal rotating speed Ω. Root retention is a passive elastic beam rigidly attached to the hub, and the reaction loads at the attachment point are extracted and added over four of them to give the hub vibratory loads. Because the AATR-II rotor system is fully articulated, three revolute joints are consecutively located between the root retention and the active blade to represent flap, lead-lag, and feathering hinges. As shown in Figure 7, the flapping and lead-lag hinges are coincident. Finally, active beams are attached to represent the AATR-II blades, and they are discretized during the analysis at least four beam elements per blade, each with 3rd-order interpolation polynomials. Thus, there are approximately 900 degrees of freedom to be solved at each time step.

In addition, to efficiently impose an Individual Blade Control (IBC)-mode sine-dwell signal with control phase variation, a series of high-voltage input is generated using the following formula:

$$V(t) = V_{\text{amplitude}} \times \cos\left\{2\pi\omega_{\text{actuation}}(t - \phi_{\text{control phase}}) + 2N_{\text{act}}\pi\phi_{\text{blade}i}\right\} \quad (4)$$

An example of the high-voltage input signal generated for an IBC-mode 3P (=3/rev) actuation with 12 divisions of control phase is shown in Figure 8. No actuation is applied for the initial 3 seconds to establish a steady-state equilibrium for the given flight condition. For each 0.5-s period of actuation, each with different control phase angle, and another 0.5-s period of no actuation is applied between them.

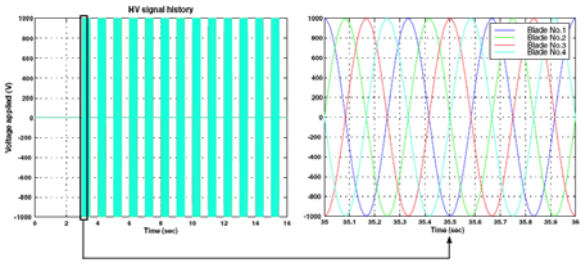

Figure 8. Example of high-voltage input generated for an IBC 3P actuation with 12 divisions of control phase angle

3. Numerical Results

3.1 Design optimization

For the design of the AATR-II blade, Table 1 [11] shows the material properties of the single crystal MFC and compares them with those of the standard MFC.

Table 1. Material properties of single crystal and standard MFC actuators

Property	Single crystal MFC	Standard MFC
E_1 [GPa]	6.2	30.3
E_2 [GPa]	11.08	15.9
G_{12} [GPa]	2.01	5.52
ν_{12}	0.23	0.31
ρ [kg/m^3]	5338	5300
d_{11} [pm/V]	1897	400
d_{12} [pm/V]	-838	-170
Thickness [$\times 10^{-4}$ m]	3.023	3.023
Electrode spacing [$\times 10^{-4}$ m]	5.334	5.334

As one can see, the single crystal MFC utilizing PMN-32%PT is more flexible and has much higher piezoelectric strain constants as compared with those of the standard MFC.

The goal of a design optimization in this section is to find the cross-section configuration which maximizes the static tip twist actuation when a certain input-voltage is given. In the present design optimization, the AATR-II blade is designed to maintain the properties of the original ATR blade. Table 2 describes the properties of the original ATR blade. Thus, the present design optimization considers various design constraints which

are given in Table 3.

Table 2. Properties of the original ATR blade

Rotor type	Fully articulated
Number of blades, b	4
Blade chord, c	0.108 m
Blade radius, R	1.397 m
Solidity, bc/πR	0.0982
Lock number	9.0
Airfoil shape	NACA 0012
Blade linear pretwist	-10 deg.
Hinge offset	7.62 cm
Root cutout	31.75 cm
Pitch axis	25% c
Elastic axis	19.6% c
Center of gravity	23.2% c
Nominal rotor speed	687.5 RPM
Mass per unit span	0.710 kg/m
1^{st} torsional frequency at nominal rotor speed	6.97/rev
Maximum strain	6327 μstrain
Twist actuation at static condtion with 2,000 V_{pp}	1.25 deg./m

Table 3. Design constraints and bounds of the design variables

Center of gravity	$0.22c \leq C.G. \leq 0.28c$
Elastic axis	$0.22c \leq E.A. \leq 0.28c$
Blade mass/length	$0.67 \leq m \leq 0.71$
1st torsional frequency	$1T \leq 5.0$/rev at 687.5 RPM
Local strain in the worst loading case	Max strain < ultimate strength of the constituent material
Web extension	$0.05c \leq Web_{ext} \leq 0.25c$
Active region starting/ ending locations	$0.0455c \leq Location \leq 0.85c$
Spar location	$0.1c \leq Spar_{loc} \leq 0.85c$

In present design optimization, as shown in Figure 4, eight design variables such as the length of the web extenstion, the spar location, two ballast weights and their locations, and the starting/ending locations of the active region, are used. In addition, Figure 9 presents the layup condition of the AATR-II blade which is based on that of the original ATR blade, but it is slightly modified.

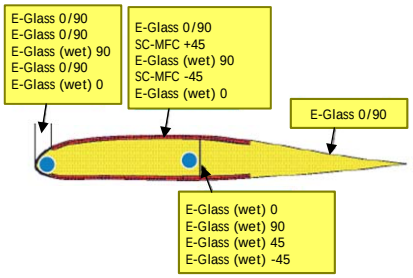

Figure 9. Layup condition of the AATR-II blade

Figure 10 illustrates the convergence history of the objective function: tip twist. The design optimization process was terminated from tolerance criteria of objective function and design variables. The optimized cross-section configuration produces the tip twist of approximately 11°, when an input-voltage is 1442 volt.

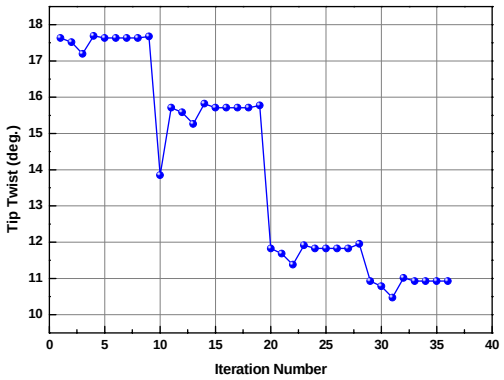

Figure 10. Convergence history of the objective function: Tip twist

The convergence history of blade properties of the AATR-II is given in Figure 11. All the properties are normalized with respect to the properties of the original ATR blade. As one can see, all the properties of the resulting blade not only satisfy all design constraints but also are similar to the properties of the original ATR blade. It is important that the resulting blade has similar properties of the original ATR blade, because the AATR-II blade is designed based on the properties of the original ATR blade.

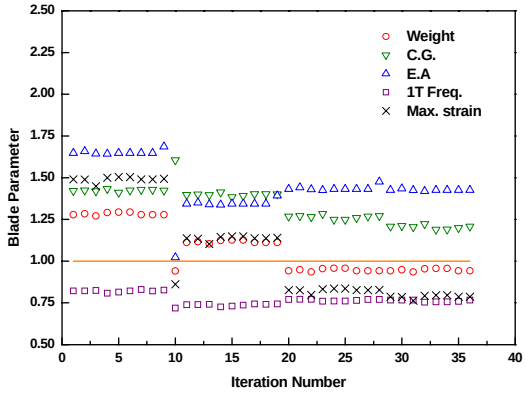

Figure 11. Convergence history of normalized blade properties

Figure 12 shows the convergence history of the blade configuration parameters. Through design optimization, for the active region, the starting location is 19% to the chord length and the ending location is 63% to the chord length. For the two ballast weights, two ballast weights are located near the nose. That is, through iteration, the

rear ballast weight moves to the leading edge. This means that the rear ballast weight is not required in order to keep the center of the gravity at near quarter point to the chord, because the single crystal MFC actuators which have high mass density are located from the fore- to after-section. For the spar, the location is approximately 40% to the chord length. As compared with the original ATR blade, the spar location is pushed forward slightly.

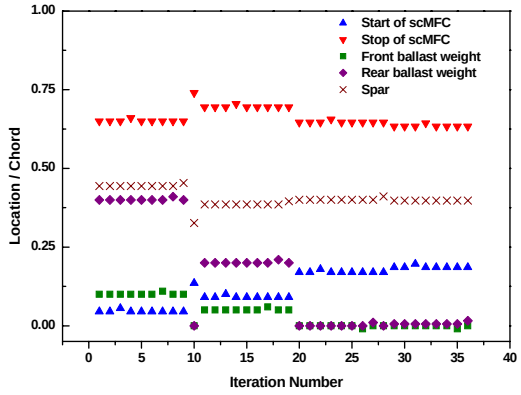

Figure 12. Convergence history of normalized blade properties

3.2 Vibratory loads reduction analysis

Since the design optimization is completed successfully, vibratory loads reduction of the optimized AATR-II blade in forward flight is investigated. Specially, the hub reaction loads of the rotor system are calculated. These vibratory loads are obtained from summation of all the loads in the four root retention elements at root retention. Figure 13 illustrates the simulated vertical component of the hub shear forces developed in the AATR-II system when 3P sine-dwell actuation is applied as given in Figure 8.

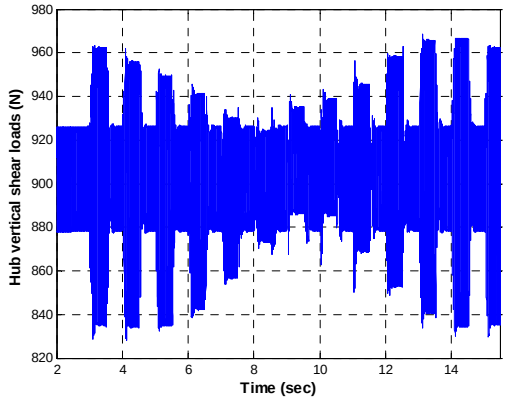

Figure 13. Simulated time history of hub vertical shear forces with 3P actuation

For this example, the amplitude of input-voltage is 200 V. In addition, the steady-state trim condition is advance ratio $\mu = 0.140$, rotor-shaft angle of attack $\alpha_s = -1°$ and thrust coefficient $C_T = 0.0066$.

This time domain analysis result can be transferred to frequency domain to investigate the magnitude of the frequency content of interest, which is 4P in the four-bladed rotor system. Figure 14 shows 4P hub shear vibratory loads with 3P, 4P and 5P actuation during the same steady-state trim condition. Here, 'baseline' represents the experimental result of the original ATR blade without actuation.

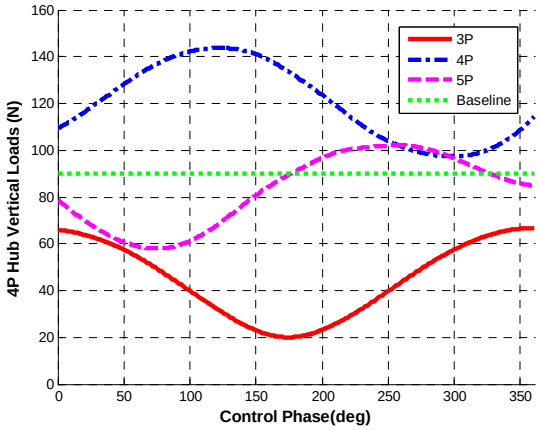

(a) Vertical

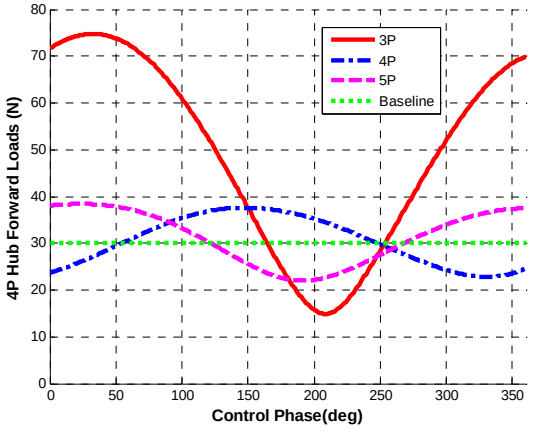

(b) Forward

Figure 14. Variation of 4P hub shear vibratory loads with 200V actuation at 3P, 4P and 5P with respect to control phase ($\mu = 0.140$, $\alpha_s = -1°$ and $C_T = 0.0066$)

As one can see, 3P actuation appears to be the most effective in reducing the hub shear vibratory loads in both cases of vertical and forward components. Particularly, as compared with the baseline value, 3P actuation with 175° control phase gives 78% reduction

of the hub vertical shear load. Furthermore, 3P actuation with 210° control phase reduces the hub forward shear load by 50%. It should be noticed that these vibratory loads reduction can be obtained when only 400 V_{pp} twist actuation of the AATR-II is imposed. To achieve this level of the vibratory loads reduction, the original ATR blade required 2,000 V_{pp} twist actuation. Since the single crystal MFC has much higher actuation performance than the AFC and the AATR-II blade is optimized, the significant vibratory loads reduction can be achieved with relatively lower input-voltage.

4. Conclusion

This work conducts the design optimization of the AATR-II blade incorporating single crystal MFC actuators, and for the optimized AATR-II blade in forward flight, the vibratory loads reduction is examined. The design optimization provides the cross-section configuration which maximizes the tip twist actuation. After the design optimization is completed successfully, using the optimized AATR-II blade, 4P hub vibratory loads are calculated and loads reduction performance is investigated. As a result, only 20% input-voltage of the original ATR blade using AFC can reduce the hub vibratory loads significantly.

Acknowledgement

This work was supported by Brain Korea 21 Project in 2007, Grant No. R01-2005-10059-0 from the Basic Research program of the Korea Science & Engineering Foundation and the KARI under KHP Dual-Use Component Development Program funded by the MOCIE.

References

[1] Bent, A. A., "Active Fiber Composites for Structural Actuation," Ph. D Thesis, Massachusetts Institute of Technology, Cambridge, MA, 1997.

[2] Wilkie, W. K., Bryant, R. G., High, J. W., Fox, R. L., Hellbaum, R. F., Jalink, A. Jr., Little, B. D., and Mirick, P. H., "Low-Cost Piezocomposite Actuator for Structural Control Applications," SPIE 7th Annual International Symposium on Smart Structures and Materials, Newport Beach, CA, 2000.

[3] Wilbur, M. L., Yeager, Jr. W. T., Wilkie, W. K., Cesnik, C. E. S., and Shin, S.-J., "Hover Testing of the NASA/ARMY/MIT Active Twist Rotor Prototype Blade," American Helicopter Society 56th Annual Forum, Virginia Beach, VA, May 2000.

[4] Cesnik, C. E. S., and Shin, S.-J., and Wilbur, M. L., "Dynamic Response of Active Twist Rotor Blades," Smart Materials and Structures-Special Issue on Rotorcraft Applications, Vol. 10, 2001, pp. 62-76.

[5] Wilbur, M. L., Mirick, P. H., Yeager, Jr. W. T., Langston, C. W., Cesnik, C. E. S., and Shin, S.-J., "Vibratory Loads Reduction Testing of the NASA/Army/MIT Active Twist Rotor," Journal of the American Helicopter Society, Vol. 47, (2), 2002, pp. 123-133.

[6] Wilbur, M. L., Yeager, Jr. W. T., and Sekula, M. K., "Further Examination of the Vibratory Loads Reduction Results form the NASA/ Army/MIT Active Twist Rotor Test," American Helicopter Society 58th Annual Forum, Montreal, Canada, June 2002.

[7] Shin, S.-J., and Cesnik, C. E. S., and Hall, S. R., "Closed-Loop Control Test of the NASA/ Army/MIT Active Twist Rotor for Vibration Reduction," American Helicopter Society 59th Annual Forum, Phoenix, AZ, May 2003.

[8] Sekula, M., K., Wilbur, M. L., and Yeager, Jr. W. T., "Aerodynamic Design Study of an Advanced Active Twist Rotor," American Helicopter Society 4th Decennial Specialist's Conference on Aeromechanics, San Francisco, CA, January 2004.

[9] Cesnik, C. E. S., Mok, J.-W., Parikh, A. S., and Shin, S.-J., "Optimization Design Framework for Integrally Twisted Helicopter Blades," 45th AIAA/ASME/ASCE/AHS/ASC Structures, Structural Dynamics and Materials Conference, Palm Springs CA, April 2004.

[10] Li, T., Scotch, A. M., Chan, H. M., Harmer, M. P., Park, S.-E., Shrout, T. R., and Michael, S. J., "Single Crystals of $Pb(Mg_{1/3}Nb_{2/3})O_3$-35 mol% $PbTiO_3$ from Polycrystalline Precursors," Journal of American Ceramic Society, Vol. 81, 1998, pp. 244-248.

[11] Park, J.-S., and Kim, J.-H., "Analytical Development of Single Crystal Macro Fiber Composite Actuators for Active Twist Rotor Blades," Smart Materials and Structures Vol. 14, 2005, pp. 745-753

[12] Wilkie, W. K., Inman, D. J., and Lloyd, J. M., "Anisotropic Laminar Piezocomposite Actuator Incorporating Machined PMN-PT Single Crystal Fibers," Journal of Intelligent material systems and structures, Vol. 17, 2006, pp.15-28

[13] TRS Ceramics, Inc. http://www.trsceramics.com

[14] Coleman, T. F., and Zhang, Y., "Optimization Toolbox for Use with MATLAB," The MathWorks, Inc., Natick, MA, 1999.

[15] Cesnik, C. E. S., and Palacios, R., "Modeling Piezocomposite Actuators Embedded in Slender

Structures," 44th AIAA/ASME/ASCE/ AHS/ASC Structures, Structural Dynamics and Materials Conference, Norfolk VA, April 2003.

[16] Bauchau, O. A., "Computational Schemes for Flexible, Nonlinear Multi-Body Systems," Multibody System Dynamics, Vol. 2, 1998, pp. 169-225.